Banana current in the inner magnetosphere observed by Van Allen Probes

Tong-Hui Wang[1,2,3], Xiao-Xin Zhang[2,3*], Fei He[4], Jing-Tian Lv[2,3], Qiu-Gang Zong[5], Hui-Shan Fu[6,7]

[1]Nanjing University of Information Science & Technology, Nanjing, China

[2]Key Laboratory of Space Weather, National Satellite Meteorological Center (National Center for Space Weather), China Meteorological Administration, Beijing, China

[3]Innovation Center for FengYun Meteorological Satellite (FYSIC), Beijing, China

[4]Key Laboratory of Earth and Planetary Physics, Institute of Geology and Geophysics, Chinese Academy of Sciences, Beijing, China

[5]Institute of Space Physics and Applied Technology, School of Earth and Space Sciences, Peking University, Beijing, China

[6]School of Space and Environment, Beihang University, Beijing, China

[7]Key Laboratory of Space Environment Monitoring and Information Processing, MIIT, Beijing, China

Corresponding author: Xiao-Xin Zhang (xxzhang@cma.gov.cn)

Key Points:

- The negative perturbation response of space currents to the geomagnetic field in the inner magnetosphere is analyzed
- Both the eastward ring current and westward ring current is asymmetric
- The vector distribution diagram of banana current density is obtained

Abstract

By using the magnetic field data from of Van Allen Probes, we analyzed the distribution characteristics of the electromagnetic environment in the inner magnetosphere on different *Dst** index and magnetic local time (MLT). Our results show that for the response of different current systems, the dawn-dusk and noon-midnight asymmetry distribution of the residual magnetic field δB increases with *Dst** index. When *Dst** < -60 nT, a 'banana'-shaped geomagnetic field negative disturbance peak region appears in the sector from midnight to dusk. Then, we

obtained the azimuthal current density and found the asymmetric internal eastward and external westward ring current. Through the vector analysis of three-dimensional current density, the current density vector distribution in the magnetic equatorial plane (MEP) is completely displayed for the first time, which directly proves the existence of banana current near r = 3.0 - 4.0 R_E during strong geomagnetic storms.

1 Introduction

The current system in the Earth's magnetosphere plays an essential role in the transport of mass and energy in the space (Olson et al., 1984; Davenport et al., 1997). The basic structure and dynamics of the primary electric current systems (e.g., magnetopause current, magnetotail current, ring current, and fild-aligned current) determine the coupling between different regions of the magnetosphere (Yu, Liemohn & Dubyagin, 2018). The ring current flowing around the Earth is one of the most important space currents in the inner magnetosphere and is usually referred as the westward ring current since the ions drift westward and electrons drift eastward. During geomagnetic storms, the ring current exhibits a significant asymmetry at different magnetic local times (MLTs), mainly manifested by the dawn-dusk asymmetry (Fukushima and Kamide, 1973; Weygand and McPherron, 2006; Chen et al., 2008; Li et al.,2011; Liu et al., 2019).

The distribution of ring current is mainly controlled by magnetic gradient and curvature radius. At the inner edge of the westward ring current, the plasma pressure rapidly decreases inward, resulting in a eastward ring current (Lui et al.,1987; 1992). Both numerical simulations (Lui et al.,1994; Ebihara et al.,2000; Liu et al.,2006; Liemohn et al.,2013; Stephens et al.,2016) and satellite observations (De Michelis et al.,1999; Le et al.,2004; Jorgensen et al.,2004; Shen et al.,2014) have confirmed the existence of the eastward ring current. Liemohn et al.(2013) also discovered asymmetry in the eastward ring current at the nightside and discussed the closure options for the eastward asymmetric current. They proposed that the current must be closed through an external westward ring current, referred to as the 'banana current'. The banana current is a current system within the magnetosphere that is completely closed within the inner magnetosphere but does not rotate around the Earth, becoming a member of the space current system (Stephens et al.,2016; Liemohn et al.,2016; Ganushkina et al.,2018).

Due to the limited spacecraft data, most studies have not fully demonstrated the distribution characteristics of the banana current. Additionally, there are few studies on the electromagnetic response in the MEP in the inner magnetosphere. The Van Allen Probes (VAP) are the first mission dedicated to the comprehensive understanding of the radiation-belt dynamics (Kletzing et al., 2013; Zanetti et

al.,2014). The twin VAP spacecrafts, VAP-A and VAP-B, have an orbital inclination of ~10° and almost identical scientific instruments (Kessel et al., 2013; Kirby et al.,2013a, 2013b; Morley et al.,2016; Spence et al.,2016; Boyd et al.,2018; Li et al., 2019). The low inclination, large elliptical orbit, high temporal resolution, and long detection period enable VAP to cover all MLT within the inner magnetosphere, which is more conducive to revealing the response mechanism of the space currents to the magnetic field disturbance in the inner magnetosphere (Kurth et al., 2015; Ali et al.,2016; Boardsen et al.,2016; Sarno et al.,2016; Yu et al.,2016; Lee et al.,2017; Yang et al.,2021). Therefore, this paper uses the VAP's magnetic field data to characterize the banana current in the inner magnetosphere.

2 Data and Methods

In this study, we use the magnetic field (1 s resolution in SM coordinates) from the fluxgate magnetometer of EMFISIS (Kletzing et al., 2013) onboard the VAP from Septemper 2012 to July 2019. To match the OMNI solar wind dataset and the geomagnetic activity index, we bined the magnetic field data to one minute. The previous studies of the large-scale ring currents in the inner magnetosphere were usually based on the solar magnetospheric (SM) cylindrical coordinate (φ, r, z) (Le et al., 2004; Jorgensen et al., 2004; Liemohn et al., 2013), where r refers to L-shell , φ refers to azimuthal angle, and z denotes the distance to the MEP. For the two VAP spacecraft, r ranges from 1.03 to 5.90 R_E, φ ranges from 0 to 2π, and z ranges from -2.0 to 2.0 R_E. Such a spatial coverage enable us to calculate the magnetic field perturbations and current densities in low-latitude region in the inner magnetosphere.

The external geomagnetic field is mainly formed due to the space current system. The perturbated magnetic field $\boldsymbol{\delta}\mathbf{B}$ can show the influence of the space current system on the geomagnetic disturbance. The perturbated magnetic field $\boldsymbol{\delta}\mathbf{B}$ can be calculated by:

$$\delta\mathbf{B} = (\delta B_{\boldsymbol{r}}, \delta B_{\boldsymbol{\varphi}}, \delta B_{\boldsymbol{z}}) = \mathbf{B}_{VAP} - \mathbf{B}_{IGRF} \qquad (1)$$

where $\mathbf{B}_{VAP}$ is the magnetic field vector measured by the VAP in nT and $\mathbf{B}_{IGRF}$ is the magnetic field vector from the international geomagnetic reference field (IGRF) in nT. Due to the curl of the ring current, the azimuthal current density, j_φ, is usually used to represent the ring current distribution (e.g., Jorgensen et al.,2004; Le et al.,2004; Liemohn et al.,2013; Stephens et al.,2016). According to the Ampere's law, j_φ in nA/m^2 is given by:

$$j_\varphi = \frac{1}{\mu_0}\left(\frac{\partial(\delta B_z)}{\partial r} - \frac{\partial(\delta B_r)}{\partial z}\right) \qquad (2)$$

where the positive value indicates westward current and negative value indicates eastward current (Jorgensen et al., 2004; Vallat et al., 2005; Carbary et al., 2012; Shen et al.,2014).

The *Dst** index ($Dst^* = Dst - 13.5(P_{dyn})^{\frac{1}{2}}$, where P_{dyn} is the solar wind dynamic pressure in nPa) is the *Dst* index that removes the effect of magnetopause current, fully reflecting the negative disturbance relationship of the space current system on the geomagnetic field (Russell et al., 1994a,1994b; Le et al., 2004). We used the *Dst** index to divide the geomagnetic disturbance into five levels (0 > *Dst** > -20 nT, -20 > *Dst** > -40 nT, -40 > *Dst** > -60 nT, -60 > *Dst** > -80 nT, *Dst** < -80 nT) to study the distribution characteristics of the perturbated magnetic field and current density.

3 Results

3.1 Statistical Patterns of δB and j_φ

Figure 1 shows the data volume, average patterns of magnetic field disturbance and current density in the MEP with a grid size of 0.5 h by 0.2 R_E in azimuthal and radial dimensions, respectively. To ensure data coverage, the radial range was limited from 2.0 to 6.0 R_E. As shown in Figure 1a, the data can cover all MLT. With the increase of disturbance level, the data coverage of non-zero value data volume can still reflect the distribution characteristics, and the single-track effect is not obvious. The main features in Figures 2b and 2c can be summarized as follows.

(1) At different levels of *Dst**, the magnetic field disturbances δB (Figure 1b) in most region of the inner magnetosphere are negative and decrease with the decline of *Dst**. As the decline of *Dst**, the distribution of δB changes from azimuthally symmetric to asymmetric, with the significant negative disturbances occur in the dusk to post-midnight sector around L-shell of 4.0. It can also be seen that as the decrease of *Dst**, the dawn-dusk and the noon-midnight asymmetry of δB become more significant.

(2) The westward ring current is mainly distributed in the region with r > 4.0 and the eastward ring current is distributed in the region with r = 2.0 - 3.5 (Figure 1c). Also, as the decline of *Dst**, the westward ring current changes from symmetric to asymmetric, and expands radially to regions closer to the Earth, in agreement with previous results (e.g., Le et al., 2004; Maltsev et al., 2004). The

strong partial ring current distributed in the dusk-midnight sector in Figure 1c results in the dawn-dusk asymmetry displayed in Figure 1b. Meanwhile, the distribution of symmetric ring currents with $Dst^* < -40$ nT demonstrates that the noon-midnight asymmetry of δB is caused by the cross-tail current.

(3) When Dst^* is larger than -60 nT, it is shown that the eastward ring currents located between L-shell of 2.0 - 3.5 are almost unchanged. At the levels of strong disturbance (e.g., $Dst^*<-60$ nT in Figure 1), however, the east ring current in the afternoon to post-midnight sector becomes significant, the geomagnetic field disturbances δB also exhibit a banana-shape in the dusk-midnight sector. This special phenomenon may be resulted from the banana current starting to appear near the nightside (Liemohn et al., 2013, 2016; Stephens et al., 2016).

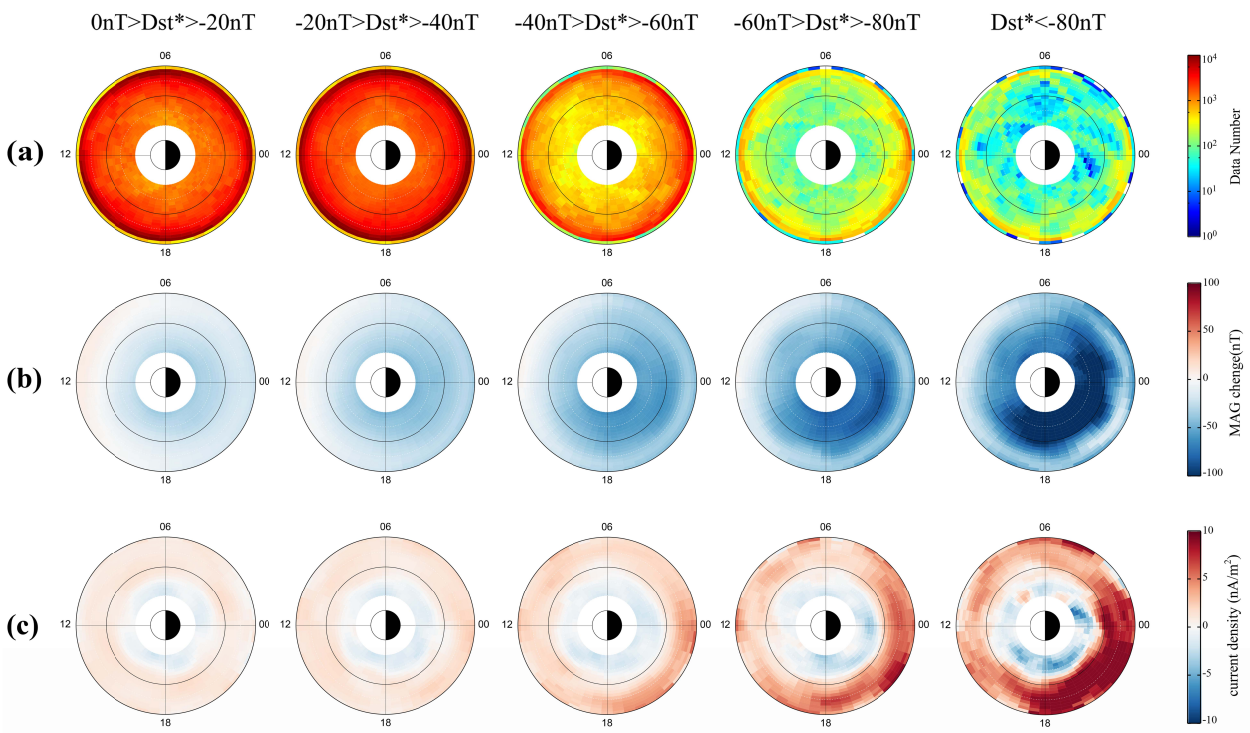

Figure 1. The data distribution with MLT × r under different geomagnetic disturbance levels, the solid black line indicates that $r = 4.0\ R_E$. (a) The non-zero value data volume. (b) The residual magnetic field δB. (c) The azimuthal current density j_φ (the positive value represents westward current, the negative value represents eastward current).

3.2 Analysis of Statistical Results of Current Density Vector

To determine whether the banana currents are always present in space or form a closure due to the radially inward movement of the westward currents in contact with the eastward currents as the magnetic storms intensify, we needed to analyze the vector distribution of the space current density. Similar to the calculation method of j_φ, the finite difference method is used to calculate the other two components of the current density, namely the radial current density j_r and the current density along the z direction j_z. Figure 2 shows the distributions of the total current density in the MEP ($\sqrt{j_\varphi^2 + j_r^2}$) overlaid with current density vector (j_φ, j_r) in three phases, namely the symmetric ring current phase (0 > Dst^* > -40 nT), the partial ring current phase (-40 > Dst^* > -60 nT), and the banana current phase (Dst^* < -60 nT).

Figure 2a shows the expected symmetric ring current phase, and the eastward and westward ring currents are disconnected in the MEP. Both are weak and almost without radial current distribution. For -40 > Dst^* > -60 nT, clear partial ring currents appear in 18-24 h MLT and expands radially inward in Figure 2b, while the eastward ring currents intensify and expands radially outward around midnight sector. The intermingling of the two types of currents results in weak radial currents near 14 h MLT and 1 h MLT, forming a weak closed annular similar to the banana current. This indicates that there should be mass transport between the two types of currents. However, unlike the banana current, the closed annular current has approximately uniform azimuthal currents on the inner side, possibly because the mass transport is not strong enough to make the eastward ring currents asymmetric.

When Dst^* < -60 nT, both the partial ring current and the eastward ring current simultaneously strengthen and expand radially. The two currents merge together, making the eastward ring current on the night side asymmetric. At the same time, the radial currents at both ends are also significantly stronger, leading to the formation of the banana current in the region from 18 h to 1 h MLT (Figure 2c). The current density in the inner region of the banana current is significantly weaker than the surrounding area. According to the Ampere's law, this region generates a

magnetic field opposite to the Earth's dipole magnetic field, which is the reason for the negative perturbation peak region of the magnetic field located at L-shell of 3 - 4 during the period of the strong geomagnetic storms.

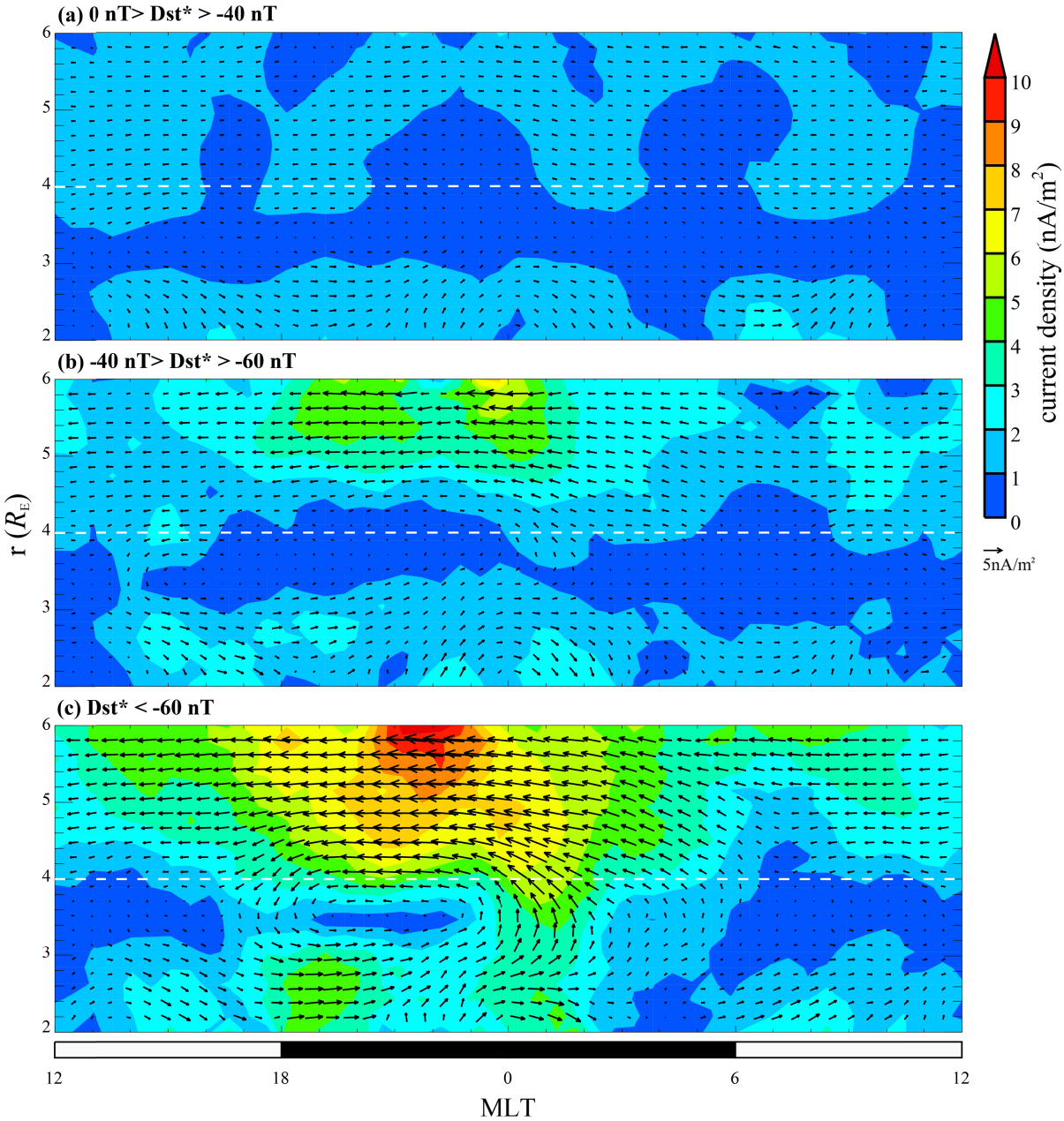

Figure 2. Current density vector distribution in the MLT × *r* plane. The magnetic disturbance intensity has (a) 0 > *Dst** > -40 nT; (b) -40 > *Dst** > -60 nT; (c) *Dst** < -60 nT. The vertical coordinate is the radial distance from the Earth in R_E. The horizontal coordinate is the MLT; the white bar below indicates the day side, and

the black color indicates the night side. The right color bar and the contour background map indicate the current density intensity, whose magnitude is kept in line with the length of the vector arrow. Where the vector direction to the right is east and to the left is west.

Figures 3a-3c show the distrubutions of current density vector in the *z*–*r* plane with the color shown the strength of the current density ($\sqrt{j_z^2 + j_r^2}$). At each disturbance level, we plot the distributions on the meridian planes with central hours of 0 h, 6 h, 12 h, and 18 h MLT, respectively. On each meridian plane, the data of 3 hours before and after the central hours are averaged. All the data are also divided into three phase as those in Figure 2. In the symmetric ring current phase in Figure 3a, Both j_z and j_r are very weak in the vast majority of regions, except for and the region at r = 2.5 - 4.5 in the souther hemisphere on the midnight-side, where a closed annular current is shown. This annular current around the midnight becomes more apprarent when the strength of the storms enhance (Figures 3b - 3c). The annular current is weaker in other meridian planes throughout the three phases.

From Figure 3c, it can be seen that the annular current continues to enhance in the southern hemisphere. However, due to the appearance of the banana current, the radial outward current density is significantly stronger than the radial inward current density on the midnight side. Thus, this becomes a radially outward part of the banana current. In contrast, the mainly radial inward current appears on the dusk side, becoming the radially inward part of the banana current. Meanwhile, vertical inward (towards the Earth) and vertical outward (away from the Earth) currents appear in the regions located at $r > 4.0$ and $|z| > 1.5$ on the dawn and dusk sides. This is due to the appearance of the partial ring current, dawn-out, and dusk-in region-2 field-aligned current from the Earth's ionosphere. Thus, the current vector behaves as dawn in and dusk out to the partial ring current.

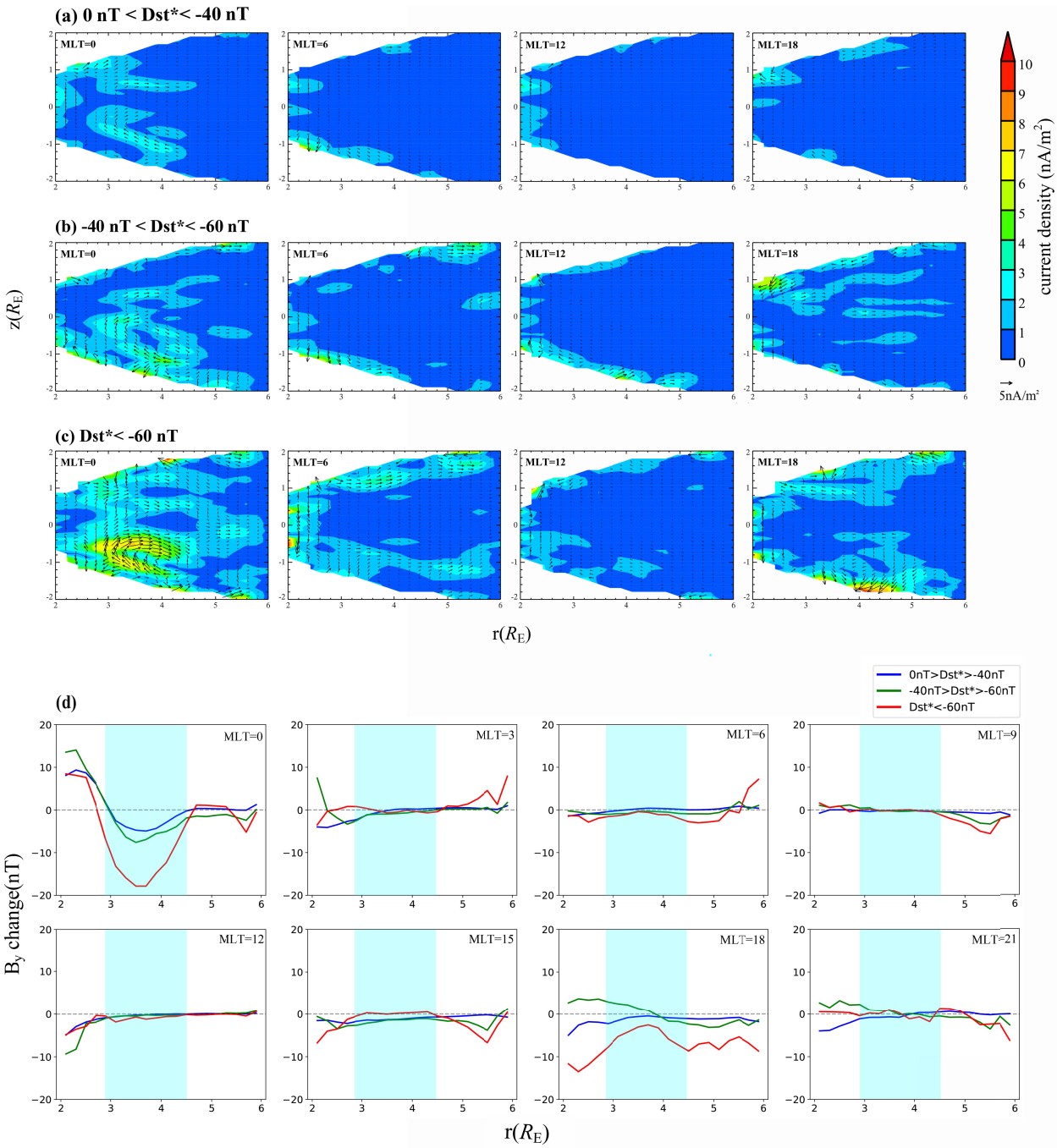

Figure 3. (a-c) Current density vector distribution in the *(z,r)* plane. The vertical coordinate is the *z*-axis, and the horizontal coordinate is the *r*-axis, both in R_E. (d) The disturbance variation of the geomagnetic B_y component with *r* at different MLT intervals. Shadows are the area of focus. The horizontal axis is the r-axis in R_E, and the vertical axis is the disturbance variation of the geomagnetic B_y component in nT.

Throughout the three phases, it can be seen that there is always an annular current on the midnight side of the *z–r* plane, this will make the *y*-component of disturbed geomagnetic field on the night side significantly weaker according to the Ampere's rule. To verify this, we plotted the distribution of the y-component of disturbed geomagnetic field at different MLT intervals. As shown in Figure 3d, the negative perturbation region of the y-component is located only in the region of r = 2.8 - 4.5 on the midnight side (0 h MLT). The magnitude of the negative disturbance in this region also increases with the enhancement of the geomagnetic disturbance. In contrast, the y-component of disturbed geomagnetic field in other MLT intervals do not have much changes with the enhancement of magnetic storms. This result further confirms the existence of the annular current around the midnight.

To show more graphically the location and characteristics of the connection between the partial ring current and the region-2 field-aligned current, we drew the distribution of the current density j_z and j_φ in the MLT-*z* plane for the L-shell range of 4-6 with Dst^* < -40 nT (Figure 4). There are apparent region-2 field-aligned currents in both the northern and southern hemispheres, and their ends are exactly at the beginning and end of the partial ring current. However, the region-2 field-aligned current and the partial ring current are stronger in the southern hemisphere than in the northern hemisphere. This indicates the phenomenon that the ring current have a weaker tilt or latitudinal shift, but does not conflict with the previous statistical results (Chen et al.,2008; Liu et al.,2019).

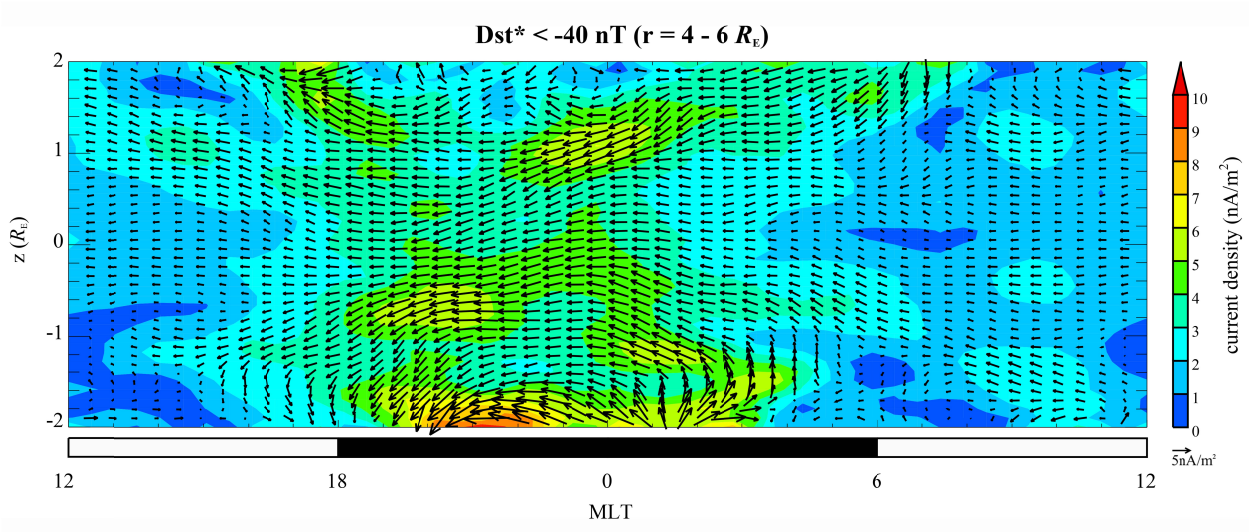

Figure 4. The current density vector distribution in the MLT × z plane. The statistical interval is r = 4.0 - 6.0 R_E, and the geomagnetic disturbance intensity is Dst^* < -40 nT. The vertical coordinate is the z-axis in R_E. The horizontal coordinate is MLT.

Conclusion

In this letter, using large amount of magnetic field data from the VAP spacecraft, a complete picture of the relationship between the space current system and geomagnetic field disturbances in the inner magnetosphere region (2.0 - 6.0 R_E) are investigated. Our main findings are summarized as follows.

1) The symmetric ring currents make the perturbated magnetic field $\boldsymbol{\delta B}$ in most region of the inner magnetosphere negative. In contrast, the cross-tail currents make the distribution of $\boldsymbol{\delta B}$ always noon-midnight asymmetry, and the partial ring currents makes $\boldsymbol{\delta B}$ exhibit significant dawn-dusk asymmetry.

2) A banana-shaped geomagnetic field negative perturbation peak area is observed in the dusk-midnight sector at r = 3.2 - 4.2 R_E only at Dst^* < -60 nT. This directly confirms the existence of the banana currents.

3) The banana current is due to the enhancement of the geomagnetic storm, and the eastward and westward ring currents are enhanced and expanded simultaneously. Thus, this makes the two currents couple together, resulting in the eastward asymmetric loop current, or the banana current.

4) We found an annular current located only around midnight, which causes a significant weakening of the y-component of the disturbed geomagnetic field on the midnight side.

The statistical results in this paper will help us further understand the circulation and distribution characteristics of the current systems in the inner magnetosphere and help us improve the inner magnetospheric geomagnetic model.

Data Availability Statement

The geomagnetic activity index data is available at: https://wdc.kugi.kyoto-u.ac.jp/wdc/Sec3.html. The VAP geomagnetic observations are available at: https://spdf.gsfc.nasa.gov/pub/data/rbsp/. The OMNI dataset is available at: https://spdf.gsfc.nasa.gov/pub/data/omni/omni_cdaweb/hro_1min/.

Acknowledgments

This work was supported by the National Natural Science Foundation of China (41931073) and the National Key R&D Program of China (2021YFA0718600).

References

Ali, A. F., Malaspina, D. M., Elkington, S. R., Jaynes, A. N., Chan, A. A., Wygant, J., & Kletzing, C. A. (2016). Electric and magnetic radial diffusion coefficients using the Van Allen probes data. Journal of Geophysical Research: Space Physics, 121, 9586–9607.https://doi.org/10.1002/2016JA023002

Boardsen, S. A., Hospodarsky, G. B., Kletzing, C. A., Engebretson, M. J., Pfaff, R. F., Wygant, J. R., et al. (2016). Survey of the frequency dependent latitudinal distribution of the fast magnetosonic wave mode from Van Allen Probes electric and magnetic field instrument and integrated science waveform receiver plasma wave analysis. Journal of Geophysical Research: Space Physics, 121, 2902–2921. https://doi.org/10.1002/2015JA021844

Boyd, A. J., Turner, D. L., Reeves, G. D., Spence, H. E., Baker, D. N., & Blake, J. B. (2018). What causes radiation belt enhancements: A survey of the Van Allen Probes Era. Geophysical Research Letters, 45, 5253–5259. https://doi.org/10.1029/2018GL077699

Carbary, J. F., N. Achilleos, and C. S. Arridge (2012), Statistical ring current of Saturn, J. Geophys. Res., 117, A06223,doi:10.1029/2011JA017472.

Chen Bo,Xu WenYao,Chen GengXiong,Du AiMin,Wu YingYan,Liu XiaoCan.2008.Latitudinal shift and tilt of the ring current during magnetic storms[J]. Chinese Science Bulletin,54(1)

Davenport G R. Chart links solar, geophysical events with impacts on space technologies[N/OL]. Eos Transactions American Geophysical Union, 1996, 77(22): 211-211, doi: 10.1029/96EO00144.

De Michelis, P., I. A. Daglis, and G. Consolini (1999), An average image of proton plasma pressure and of current systems in the equatorial plane derived from AMPTE/CCE-CHEM measurements, J. Geophys. Res., 104(A12), 28,615–28,624, doi:10.1029/1999JA900310.

Ebihara, Y. and Ejiri, M.: 2000, 'Simulation Study on Fundamental Properties of the Storm-time Ring Current', J. Geophys. Res., 105, 15 843.

Fukushima, N., & Kamide, Y. （1973）. Partial ring current models for worldwide geomagnetic disturbances. Reviews of Geophysics, 11（4）,795–853. https://doi.org/10.1029/RG011i004p00795

Ganushkina, N. Y., Liemohn, M. W.,& Dubyagin, S. (2018). Current systems in the Earth′s magnetosphere. Reviews of Geophysics, 56, 309–332.https://doi.org/10.1002/2017RG000590

Jorgensen, A. M., H. E. Spence, W. J. Hughes, and H. J. Singer (2004), A statistical study of the global structure of the ring current, J. Geophys. Res., 109, A12204, doi:10.1029/2003JA010090.

Kessel, R. L., Fox, N. J., & Weiss, M. (2013). The Radiation Belt Storm Probes (RBSP) and space weather. Space Science Reviews, 179(1-4), 531–543. https://doi.org/10.1007/s11214-012-9953-6

Kirby, K., Artis, D., Bushman, S., Butler, M., Conde, R., Cooper, S., ... Williams, B. (2013a). Radiation Belt Storm Probes—Observatory and environments. Space Science Reviews, 179(1-4), 59–125. https://doi.org/10.1007/s11214-012-9949-2

Kirby K., & Stratton, J. (2013b). Van Allen Probes: Successful launch campaign and early operations exploring Earth′s radiation belts. In Proceedings of the 2013 IEEE Aerospace Conference.

Kletzing, C. A. , Kurth, W. S. , Acuna, M. , Macdowall, R. J. , Torbert, R. B. , & Averkamp, T. , et al. 2013. The electric and magnetic field instrument suite and integrated science (EMFISIS) on RBSP. *Space Science Reviews*. 179. 10.1007/s11214-013-9993-6.

Le, G., Russell, C. T., & Takahashi, K. (2004). Morphology of the ring current derived from magnetic field observations. Annales de Geophysique,22（4）,1267–1295. sref:1432–0576/ag/2004–22-1267, https://doi.org/10.5194/angeo-22-1267-2004

Lee, J., Kim, K.-C., Giuseppe, R.,Ukhorskiy, S., Sibeck, D., Kessel, R., …Lee, J. (2018). Space weather operation at KASI with Van Allen Probes beacon signals. Space Weather, 16, 108–120. https://doi.org/10.1002/2017SW001726

Li, H., C. Wang, and J. R. Kan (2011), Contribution of the partial ring current to the SYMH index during magnetic storms, J. Geophys. Res., 116, A11222, doi:10.1029/2011JA016886.

Li, W., & Hudson, M. K. 2019. Earth's Van Allen radiation belts: From discovery to the Van Allen Probes era. Journal of Geophysical Research: Space Physics, 124, 8319– 8351. https://doi.org/10.1029/2018JA025940

Liemohn, M. W., N. Y. Ganushkina, R. Ilie,and D. T. Welling (2016), Challenges associated with near-Earth nightside current, J. Geophys. Res. Space Physics,121, 6763–6768, doi:10.1002/2016JA022948.

Liemohn, M. W., N. Y. Ganushkina, R. M. Katus, D. L. De Zeeuw, and D. T. Welling (2013), The magnetospheric banana current, J. Geophys. Res. Space Physics, 118, 1009–1021,doi:10.1002/jgra.50153.

Liu X, Liu W L. 2014. A new plasmapause location model based on THEMIS observations. Science China: Earth Sciences, doi: 10.1007/s11430- 014-4844-1

Liu, B.-J., Zhang, X.-X., He, F., & Zong,Q.-G. （2019）. The magnetic local time distribution of storm geomagnetic field disturbance under different conditions of solar wind and interplanetary magnetic field. Journal of Geophysical Research: Space Physics, 124,2656–2667.https://doi.org/10.1029/2018JA026287

Liu, S., M. W. Chen, M. Schulz, and L. R. Lyons (2006), Initial simulation results of storm-time ring current in a self_x0002_consistent magnetic field model, J. Geophys. Res., 111, A04225, doi:10.1029/2005JA011194.

Lui, A. T. Y., McEntire, R. W., and Krimigis, S. M.: Evolution of the ring current during two geomagnetic storms, J. Geophys.Res., 92, 7459–7470, 1987.

Lui, A. T. Y., and D.C. Hamilton, Radial profiles of quiet time magnetospheric parameters, J. Geophys. Res., 97, 19,325, 1992.

Lui, A. T. Y., H. E. Spence, and D. P. Stern, Empirical modelling of the quiet time nightside magnetosphere, d. Geophys, Res., 99, 151, 1994.

Lv, J.-T., Zhang, X.-X., He, F., & Lin, R.-L. (2022). A statistical model of inner magnetospheric electron density: Van Allen Probes observations. Space Weather, 20, e2022SW003182. https://doi.org/10.1029/2022SW003182

Maltsev, Y. P. （2004）, Points of controversy in the study of magnetic storms, Space Sci. Rev., 110, 227–267.

Morley, S. K., Sullivan, J. P., Henderson, M. G., Blake, J. B., & Baker, D. N. (2016). The Global Positioning System constellation as a space weather monitor: Comparison of electron measurements with Van Allen Probes data. Space Weather, 14, 76–92. https://doi.org/10.1002/2015SW001339

Ohtani, S., Ebihara, Y., & Singer, H. J. （2007）. Storm-time magnetic configurations at geosynchronous orbit: Comparison between the main and recovery phases. Journal of Geophysical Research, 112, A05202. https://doi.org/10.1029/2006JA011959

Olson, W. P. 1984, Introduction to the topology of magnetospheric current system, in Magnetospheric Current, Geophys. Monogr. Ser., vol. 28, edited by T. A. Potemra, pp. 49–66, AGU, Washington, D. C.

Russel, C. T., Ginskey, M., and Petrinec, S. M.(1994a).Sudden impulses at low-latitude stations: Steady state response for northward interplanetary magnetic fifield, J. Geophys. Res., 99, 253–261,.

Russel, C. T., Ginskey, M., and Petrinec, S. M.(1994b).Sudden impulses at low-latitude stations: Steady state response for southward in terplanetary magnetic fifield, J. Geophys. Res., 99, 13 403–13 408.

Sarno-Smith, L. K., Larsen, B. A., Skoug, R. M., Liemohn, M. W., Breneman, A., Wygant, J. R., & Thomsen, M. F. (2016). Spacecraft surface charging within geosynchronous orbit observed by the Van Allen Probes. Space Weather, 14, 151–164. https://doi.org/10.1002/2015SW001345

Shen, C., et al. (2014), Direct calculation of the ring current distribution and magnetic structure seen by Cluster during geomagnetic storms, J. Geophys. Res. Space Physics, 119, 2458–2465, doi:10.1002/2013JA019460.

Spence, H. E., Reeves, G. D., Baker, D. N., Blake, J. B., Bolton, M., Bourdarie, S., et al. (2013). Science goals and overview of the Energetic Particle, Composition, and Thermal Plasma (ECT) Suite on NASA's Radiation Belt Storm Probes (RBSP) Mission. Space Science Reviews,179(1-4), 311–336. https://doi.org/10.1007/s11214-013-0007-5

Stephens, G. K., M. I. Sitnov,A. Y. Ukhorskiy, E. C. Roelof,N. A. Tsyganenko, and G. Le (2016),Empirical modeling of the storm time innermost magnetosphere using Van Allen Probes and THEMIS data:Eastward and banana currents,J. Geophys. Res. SpacePhysics, 121, 157–170,doi:10.1002/2015JA021700.

Weygand, J. M., and R. L. McPherron （2006）, Dependence of ring current asymmetry on storm phase, J. Geophys. Res., 111, A11221, doi:10.1029/2006JA011808.

Yang, X., & Wang, L. (2021). A study of the performances of widely used external magnetic field models in the outer zone of the Earth's radiation belts by comparing the field observations from Van Allen Probe-A and the model estimations. Space Weather, 19, e2021SW002722. https://doi.org/10.1029/2021SW002722

Yu, J., L. Y. Li, J. B. Cao, G. D. Reeves,D. N. Baker, and H. Spence (2016), The influences of solar wind pressure and interplanetary magnetic field on global

magnetic field and outer radiation belt electrons, Geophys. Res. Lett., 43,7319–7327, doi:10.1002/2016GL069029.

Zanetti, L. J., B. H. Mauk, N. J. Fox,R. J. Barnes, M. Weiss, T. S. Sotirelis,N.-E. Raouafi, R. L. Kessel, and H. N. Becker (2014), The Evolving Space Weather System—Van Allen Probes Contribution, Space Weather, 12,577–581,doi:10.1002/2014SW001108.

Figure1.

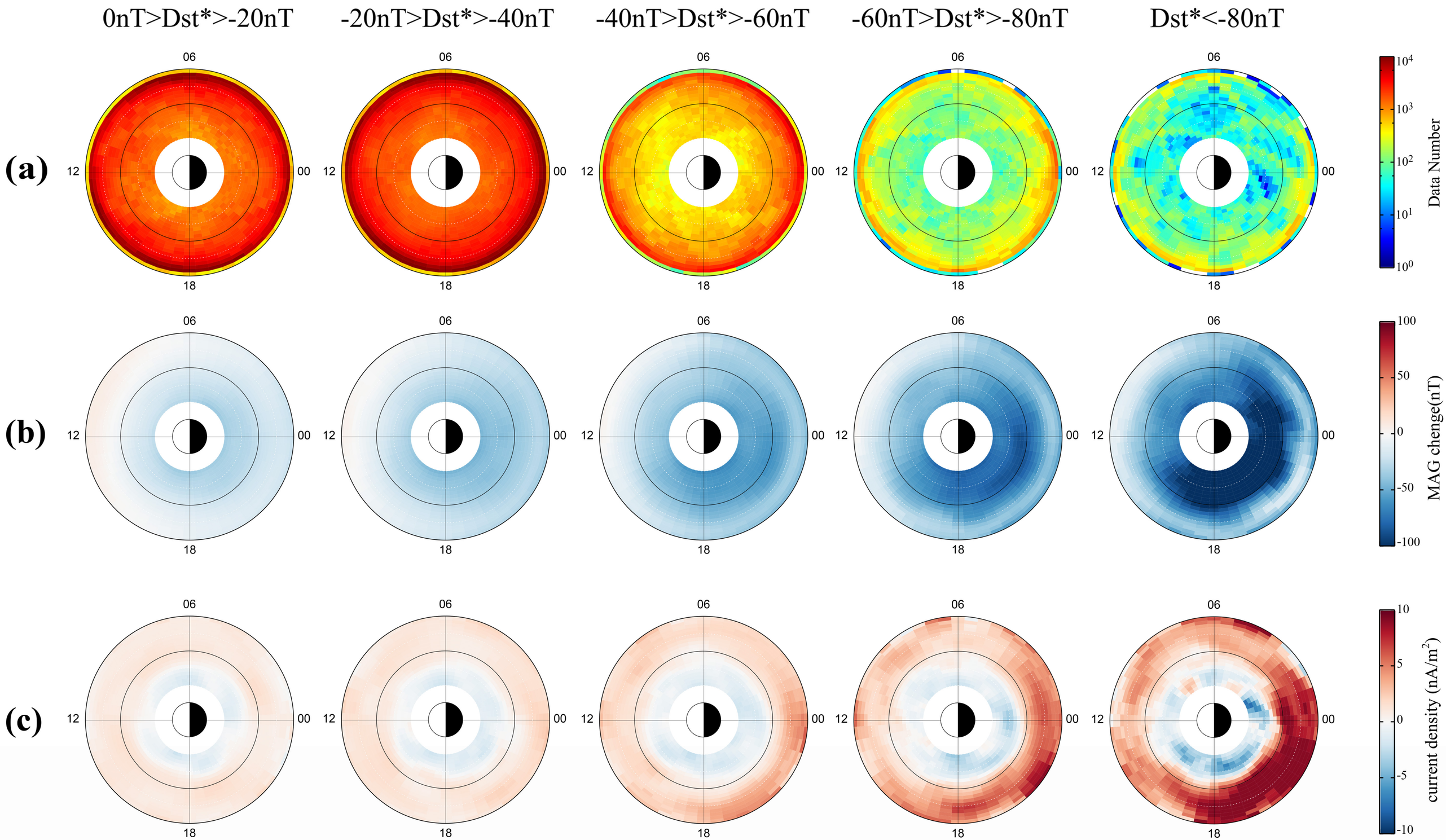
0nT>Dst*>-20nT
-20nT>Dst*>-40nT
-40nT>Dst*>-60nT
-60nT>Dst*>-80nT
Dst*<-80nT
(a)
(b)
(c)
06
12
00
18
Data Number
MAG chenge(nT)
current density (nA/m2)

Figure2.

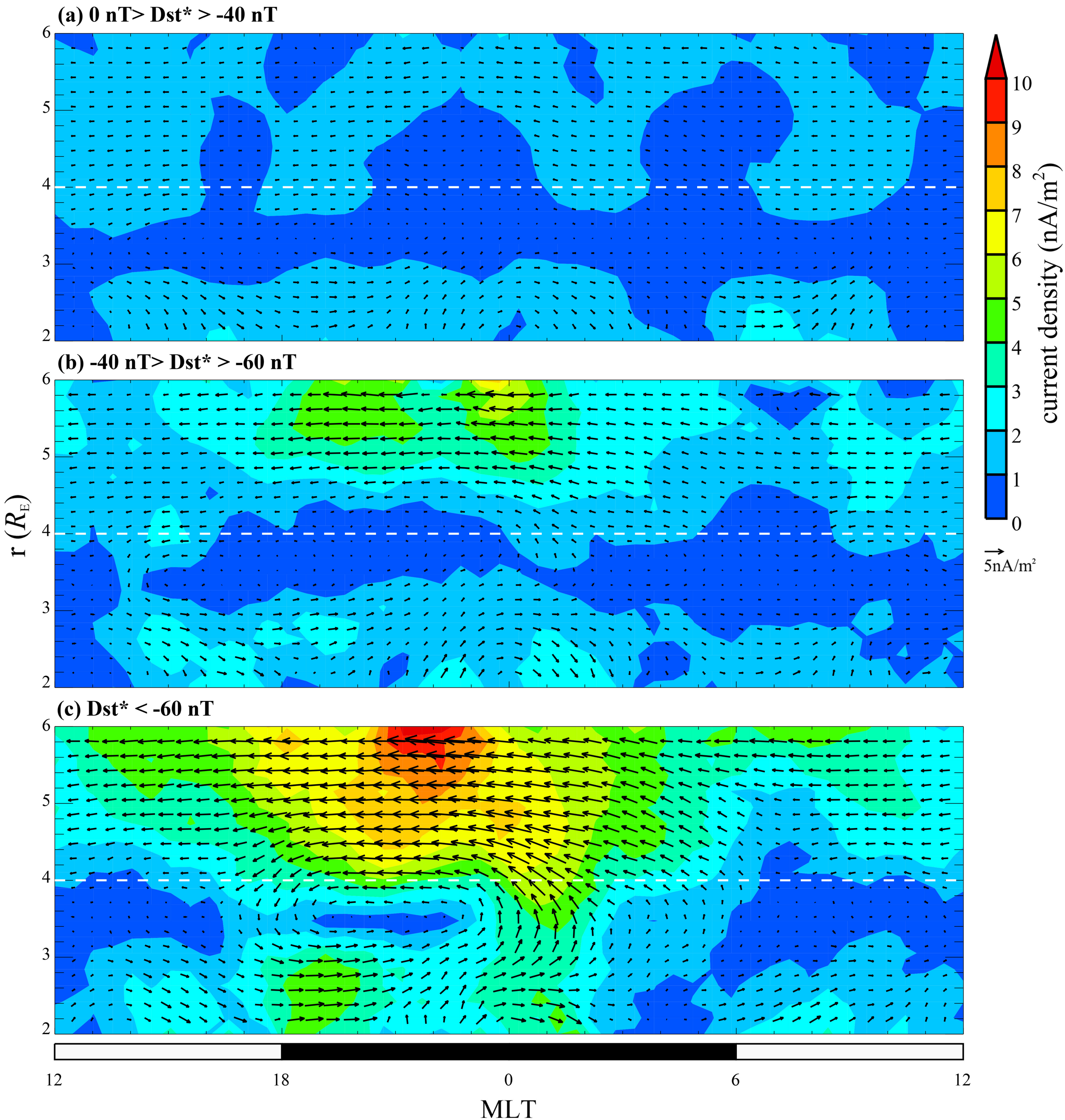
(a) 0 nT> Dst* > -40 nT
(b) -40 nT> Dst* > -60 nT
(c) Dst* < -60 nT
r (R_E)
6
5
4
3
2
12
18
0
6
12
MLT
10
9
8
7
6
5
4
3
2
1
0
current density (nA/m^2)
5nA/m^2

Figure3.

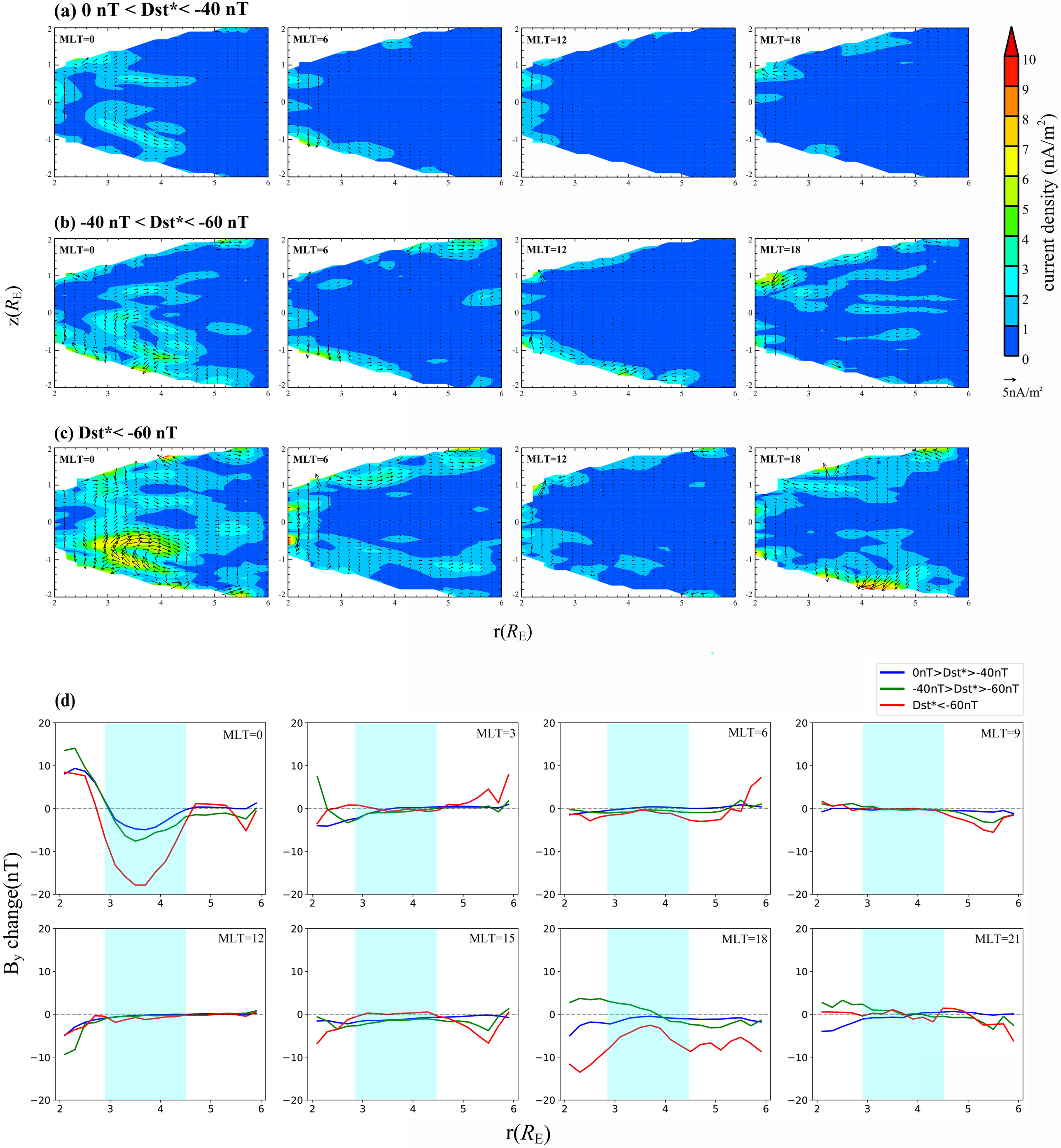
(a) 0 nT < Dst*< -40 nT
(b) -40 nT < Dst*< -60 nT
(c) Dst*< -60 nT
MLT=0
MLT=6
MLT=12
MLT=18
z(R_E)
r(R_E)
current density (nA/m^2)
5nA/m²
(d)
0nT>Dst*>-40nT
-40nT>Dst*>-60nT
Dst*<-60nT
MLT=0
MLT=3
MLT=6
MLT=9
MLT=12
MLT=15
MLT=18
MLT=21
B_y change(nT)
r(R_E)

Figure4.

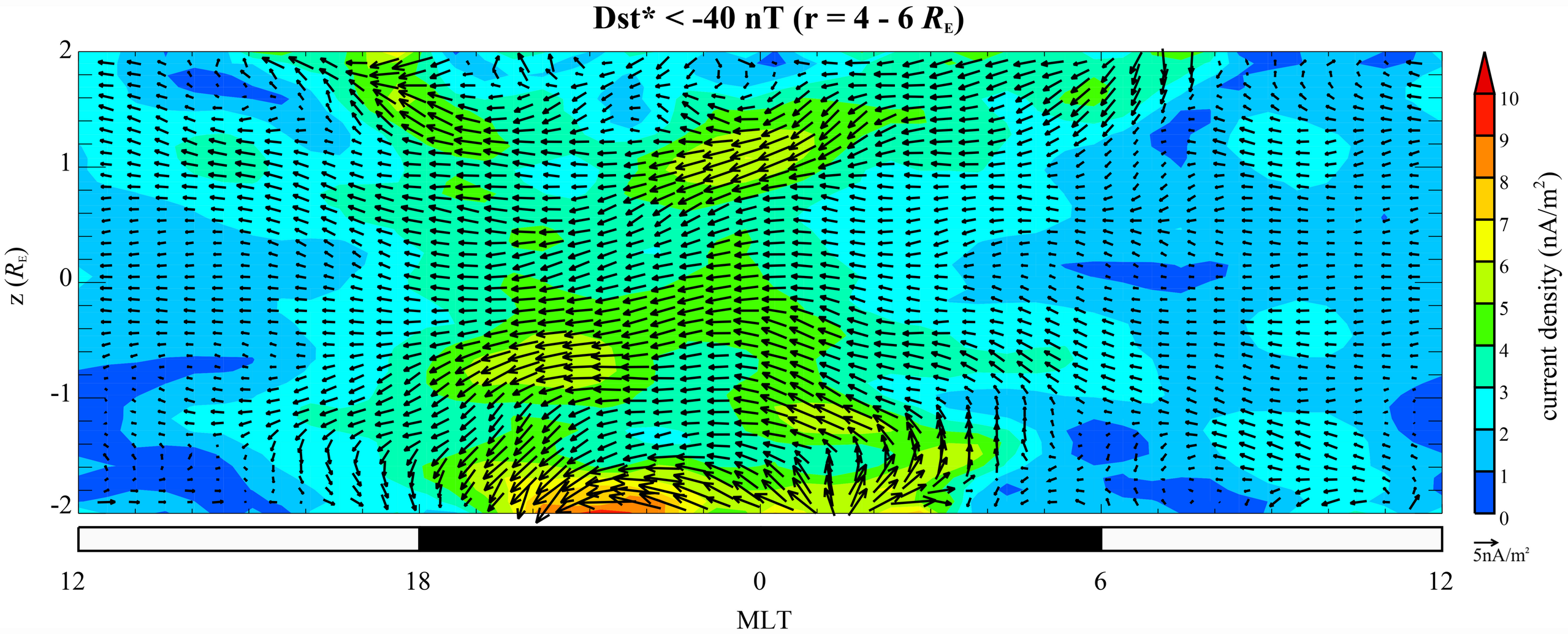
Dst* < -40 nT (r = 4 - 6 R_E)
z (R_E)
2
1
0
-1
-2
12
18
0
6
12
MLT
current density (nA/m^2)
10
9
8
7
6
5
4
3
2
1
0
5nA/m^2